

Proceedings of the 12th International Conference on
Computational Fluid Dynamics in the Oil & Gas,
Metallurgical and Process Industries

Progress in Applied CFD – CFD2017



SINTEF Proceedings

Editors:

Jan Erik Olsen and Stein Tore Johansen

Progress in Applied CFD – CFD2017

Proceedings of the 12th International Conference on Computational Fluid Dynamics
in the Oil & Gas, Metallurgical and Process Industries

SINTEF Academic Press

SINTEF Proceedings no 2

Editors: Jan Erik Olsen and Stein Tore Johansen

Progress in Applied CFD – CFD2017

Selected papers from 10th International Conference on Computational Fluid Dynamics in the Oil & Gas, Metallurgical and Process Industries

Key words:

CFD, Flow, Modelling

Cover, illustration: Arun Kamath

ISSN 2387-4295 (online)

ISBN 978-82-536-1544-8 (pdf)

© Copyright SINTEF Academic Press 2017

The material in this publication is covered by the provisions of the Norwegian Copyright Act. Without any special agreement with SINTEF Academic Press, any copying and making available of the material is only allowed to the extent that this is permitted by law or allowed through an agreement with Kopinor, the Reproduction Rights Organisation for Norway. Any use contrary to legislation or an agreement may lead to a liability for damages and confiscation, and may be punished by fines or imprisonment

SINTEF Academic Press

Address: Forskningsveien 3 B
 PO Box 124 Blindern
 N-0314 OSLO

Tel: +47 73 59 30 00

Fax: +47 22 96 55 08

www.sintef.no/byggforsk

www.sintefbok.no

SINTEF Proceedings

SINTEF Proceedings is a serial publication for peer-reviewed conference proceedings on a variety of scientific topics.

The processes of peer-reviewing of papers published in SINTEF Proceedings are administered by the conference organizers and proceedings editors. Detailed procedures will vary according to custom and practice in each scientific community.

PREFACE

This book contains all manuscripts approved by the reviewers and the organizing committee of the 12th International Conference on Computational Fluid Dynamics in the Oil & Gas, Metallurgical and Process Industries. The conference was hosted by SINTEF in Trondheim in May/June 2017 and is also known as CFD2017 for short. The conference series was initiated by CSIRO and Phil Schwarz in 1997. So far the conference has been alternating between CSIRO in Melbourne and SINTEF in Trondheim. The conferences focuses on the application of CFD in the oil and gas industries, metal production, mineral processing, power generation, chemicals and other process industries. In addition pragmatic modelling concepts and bio-mechanical applications have become an important part of the conference. The papers in this book demonstrate the current progress in applied CFD.

The conference papers undergo a review process involving two experts. Only papers accepted by the reviewers are included in the proceedings. 108 contributions were presented at the conference together with six keynote presentations. A majority of these contributions are presented by their manuscript in this collection (a few were granted to present without an accompanying manuscript).

The organizing committee would like to thank everyone who has helped with review of manuscripts, all those who helped to promote the conference and all authors who have submitted scientific contributions. We are also grateful for the support from the conference sponsors: ANSYS, SFI Metal Production and NanoSim.

Stein Tore Johansen & Jan Erik Olsen



Organizing committee:

Conference chairman: Prof. Stein Tore Johansen

Conference coordinator: Dr. Jan Erik Olsen

Dr. Bernhard Müller

Dr. Sigrid Karstad Dahl

Dr. Shahriar Amini

Dr. Ernst Meese

Dr. Josip Zoric

Dr. Jannike Solsvik

Dr. Peter Witt

Scientific committee:

Stein Tore Johansen, SINTEF/NTNU

Bernhard Müller, NTNU

Phil Schwarz, CSIRO

Akio Tomiyama, Kobe University

Hans Kuipers, Eindhoven University of Technology

Jinghai Li, Chinese Academy of Science

Markus Braun, Ansys

Simon Lo, CD-adapco

Patrick Segers, Universiteit Gent

Jiyuan Tu, RMIT

Jos Derksen, University of Aberdeen

Dmitry Eskin, Schlumberger-Doll Research

Pär Jönsson, KTH

Stefan Pirker, Johannes Kepler University

Josip Zoric, SINTEF

CONTENTS

PRAGMATIC MODELLING	9
On pragmatism in industrial modeling. Part III: Application to operational drilling	11
CFD modeling of dynamic emulsion stability	23
Modelling of interaction between turbines and terrain wakes using pragmatic approach	29
FLUIDIZED BED	37
Simulation of chemical looping combustion process in a double looping fluidized bed reactor with cu-based oxygen carriers.....	39
Extremely fast simulations of heat transfer in fluidized beds.....	47
Mass transfer phenomena in fluidized beds with horizontally immersed membranes	53
A Two-Fluid model study of hydrogen production via water gas shift in fluidized bed membrane reactors	63
Effect of lift force on dense gas-fluidized beds of non-spherical particles	71
Experimental and numerical investigation of a bubbling dense gas-solid fluidized bed	81
Direct numerical simulation of the effective drag in gas-liquid-solid systems	89
A Lagrangian-Eulerian hybrid model for the simulation of direct reduction of iron ore in fluidized beds.....	97
High temperature fluidization - influence of inter-particle forces on fluidization behavior	107
Verification of filtered two fluid models for reactive gas-solid flows	115
BIOMECHANICS.....	123
A computational framework involving CFD and data mining tools for analyzing disease in carotid artery	125
Investigating the numerical parameter space for a stenosed patient-specific internal carotid artery model.....	133
Velocity profiles in a 2D model of the left ventricular outflow tract, pathological case study using PIV and CFD modeling.....	139
Oscillatory flow and mass transport in a coronary artery.....	147
Patient specific numerical simulation of flow in the human upper airways for assessing the effect of nasal surgery.....	153
CFD simulations of turbulent flow in the human upper airways	163
OIL & GAS APPLICATIONS	169
Estimation of flow rates and parameters in two-phase stratified and slug flow by an ensemble Kalman filter	171
Direct numerical simulation of proppant transport in a narrow channel for hydraulic fracturing application	179
Multiphase direct numerical simulations (DNS) of oil-water flows through homogeneous porous rocks	185
CFD erosion modelling of blind tees	191
Shape factors inclusion in a one-dimensional, transient two-fluid model for stratified and slug flow simulations in pipes	201
Gas-liquid two-phase flow behavior in terrain-inclined pipelines for wet natural gas transportation	207

NUMERICS, METHODS & CODE DEVELOPMENT	213
Innovative computing for industrially-relevant multiphase flows	215
Development of GPU parallel multiphase flow solver for turbulent slurry flows in cyclone.....	223
Immersed boundary method for the compressible Navier–Stokes equations using high order summation-by-parts difference operators	233
Direct numerical simulation of coupled heat and mass transfer in fluid-solid systems	243
A simulation concept for generic simulation of multi-material flow, using staggered Cartesian grids.....	253
A cartesian cut-cell method, based on formal volume averaging of mass, momentum equations.....	265
SOFT: a framework for semantic interoperability of scientific software	273
 POPULATION BALANCE	 279
Combined multifluid-population balance method for polydisperse multiphase flows	281
A multifluid-PBE model for a slurry bubble column with bubble size dependent velocity, weight fractions and temperature.....	285
CFD simulation of the droplet size distribution of liquid-liquid emulsions in stirred tank reactors	295
Towards a CFD model for boiling flows: validation of QMOM predictions with TOPFLOW experiments	301
Numerical simulations of turbulent liquid-liquid dispersions with quadrature-based moment methods.....	309
Simulation of dispersion of immiscible fluids in a turbulent couette flow	317
Simulation of gas-liquid flows in separators - a Lagrangian approach.....	325
CFD modelling to predict mass transfer in pulsed sieve plate extraction columns	335
 BREAKUP & COALESCENCE	 343
Experimental and numerical study on single droplet breakage in turbulent flow	345
Improved collision modelling for liquid metal droplets in a copper slag cleaning process	355
Modelling of bubble dynamics in slag during its hot stage engineering.....	365
Controlled coalescence with local front reconstruction method	373
 BUBBLY FLOWS	 381
Modelling of fluid dynamics, mass transfer and chemical reaction in bubbly flows	383
Stochastic DSMC model for large scale dense bubbly flows.....	391
On the surfacing mechanism of bubble plumes from subsea gas release.....	399
Bubble generated turbulence in two fluid simulation of bubbly flow	405
 HEAT TRANSFER	 413
CFD-simulation of boiling in a heated pipe including flow pattern transitions using a multi-field concept	415
The pear-shaped fate of an ice melting front	423
Flow dynamics studies for flexible operation of continuous casters (flow flex cc).....	431
An Euler-Euler model for gas-liquid flows in a coil wound heat exchanger.....	441
 NON-NEWTONIAN FLOWS.....	 449
Viscoelastic flow simulations in disordered porous media	451
Tire rubber extrudate swell simulation and verification with experiments	459
Front-tracking simulations of bubbles rising in non-Newtonian fluids.....	469
A 2D sediment bed morphodynamics model for turbulent, non-Newtonian, particle-loaded flows.....	479

METALLURGICAL APPLICATIONS.....	491
Experimental modelling of metallurgical processes	493
State of the art: macroscopic modelling approaches for the description of multiphysics phenomena within the electroslag remelting process	499
LES-VOF simulation of turbulent interfacial flow in the continuous casting mold	507
CFD-DEM modelling of blast furnace tapping	515
Multiphase flow modelling of furnace tapholes	521
Numerical predictions of the shape and size of the raceway zone in a blast furnace.....	531
Modelling and measurements in the aluminium industry - Where are the obstacles?	541
Modelling of chemical reactions in metallurgical processes.....	549
Using CFD analysis to optimise top submerged lance furnace geometries	555
Numerical analysis of the temperature distribution in a martensic stainless steel strip during hardening.....	565
Validation of a rapid slag viscosity measurement by CFD.....	575
Solidification modeling with user defined function in ANSYS Fluent.....	583
Cleaning of polycyclic aromatic hydrocarbons (PAH) obtained from ferroalloys plant.....	587
Granular flow described by fictitious fluids: a suitable methodology for process simulations	593
A multiscale numerical approach of the dripping slag in the coke bed zone of a pilot scale Si-Mn furnace.....	599
INDUSTRIAL APPLICATIONS	605
Use of CFD as a design tool for a phosphoric acid plant cooling pond	607
Numerical evaluation of co-firing solid recovered fuel with petroleum coke in a cement rotary kiln: Influence of fuel moisture	613
Experimental and CFD investigation of fractal distributor on a novel plate and frame ion-exchanger	621
COMBUSTION	631
CFD modeling of a commercial-size circle-draft biomass gasifier.....	633
Numerical study of coal particle gasification up to Reynolds numbers of 1000.....	641
Modelling combustion of pulverized coal and alternative carbon materials in the blast furnace raceway	647
Combustion chamber scaling for energy recovery from furnace process gas: waste to value	657
PACKED BED.....	665
Comparison of particle-resolved direct numerical simulation and 1D modelling of catalytic reactions in a packed bed	667
Numerical investigation of particle types influence on packed bed adsorber behaviour	675
CFD based study of dense medium drum separation processes	683
A multi-domain 1D particle-reactor model for packed bed reactor applications.....	689
SPECIES TRANSPORT & INTERFACES	699
Modelling and numerical simulation of surface active species transport - reaction in welding processes	701
Multiscale approach to fully resolved boundary layers using adaptive grids.....	709
Implementation, demonstration and validation of a user-defined wall function for direct precipitation fouling in Ansys Fluent.....	717

FREE SURFACE FLOW & WAVES	727
Unresolved CFD-DEM in environmental engineering: submarine slope stability and other applications.....	729
Influence of the upstream cylinder and wave breaking point on the breaking wave forces on the downstream cylinder	735
Recent developments for the computation of the necessary submergence of pump intakes with free surfaces	743
Parallel multiphase flow software for solving the Navier-Stokes equations	752
 PARTICLE METHODS	 759
A numerical approach to model aggregate restructuring in shear flow using DEM in Lattice-Boltzmann simulations	761
Adaptive coarse-graining for large-scale DEM simulations.....	773
Novel efficient hybrid-DEM collision integration scheme.....	779
Implementing the kinetic theory of granular flows into the Lagrangian dense discrete phase model.....	785
Importance of the different fluid forces on particle dispersion in fluid phase resonance mixers	791
Large scale modelling of bubble formation and growth in a supersaturated liquid.....	798
 FUNDAMENTAL FLUID DYNAMICS	 807
Flow past a yawed cylinder of finite length using a fictitious domain method	809
A numerical evaluation of the effect of the electro-magnetic force on bubble flow in aluminium smelting process.....	819
A DNS study of droplet spreading and penetration on a porous medium.....	825
From linear to nonlinear: Transient growth in confined magnetohydrodynamic flows.....	831

ON THE SURFACING MECHANISM OF BUBBLE PLUMES FROM SUBSEA GAS RELEASE

Jan Erik OLSEN & Paal SKJETNE

SINTEF Materials and Chemistry, 7465 Trondheim, NORWAY

* E-mail: jan.e.olsen@sintef.no

ABSTRACT

A subsea release of gas poses a risk to humans and assets at the surface. Assessing this risk requires knowledge on how much gas reaches the surface and how it is distributed at the surface. This can be estimated by various modelling techniques, e.g. CFD. Reported surfacing flux can then be fed into a CFD model for atmospheric dispersion calculations. This paper briefly discusses how the surface flux can be calculated by CFD, but primarily focuses on the surfacing characteristics and discusses how the surface flux can be reported and issues related to this.

Keywords: CFD, bubbly flows, subsea gas release

NOMENCLATURE

Greek Symbols

- ρ Mass density, [kg/m³].
 σ Standard deviation, [m].

Latin Symbols

- a Characteristic length, [m].
 \mathbf{F} Force, [N/m].
 \mathbf{g} Gravitational acceleration, [m/s²].
 J Gas flux, [kg/m²s].
 \dot{m} mass rate, [kg/s].
 r radius, [m].
 t Time, [s].
 \mathbf{u} Velocity, [m/s].

Sub/superscripts

- θ Centre
 b Bubble.
 D Drag.
 VM Virtual mass.
 tot Total

INTRODUCTION

A subsea gas release of hydrocarbons such as methane presents a risk of fire and explosions when the gas emerges into the atmosphere. Risk assessments are normally based on modelling of atmospheric dispersion of hazardous gases. Modelling of atmospheric dispersion

relies on a boundary condition which prescribes the flux of gas escaping from the ocean into the atmosphere. This flux will vary in time and position, although many assume it to be constant. In this work we try to characterize a surfacing profile and provide guidelines on how this can be represented as a boundary condition in atmospheric dispersion models.

The ocean surface boundary condition for atmospheric simulations can be provided by a subsea model of the bubble plume. Different modelling concepts are available for this. Traditionally, classical plume integral models, which are computationally fast, have been applied for this (Johansen, 2000; Morton *et al.*, 1956; Zheng & Yapa, 2002). These are based on a series of assumptions and calibration coefficients, but still have proven to reproduce experimental results at least at smaller scales. Transient 3-dimensional CFD modelling of these plumes are computationally expensive due to the large length scales involved, but they rely on fewer assumptions – especially in the surfacing region. The authors of this work have contributed to the development of a CFD model for bubble plumes from subsea gas releases (Cloete *et al.*, 2009; Olsen *et al.*, 2017).

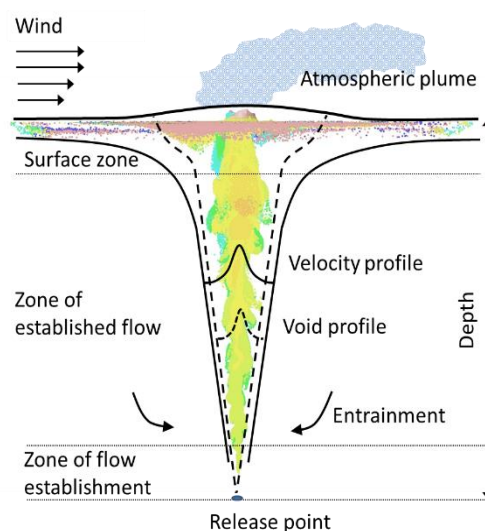


Figure 1: Illustration of subsea gas release.

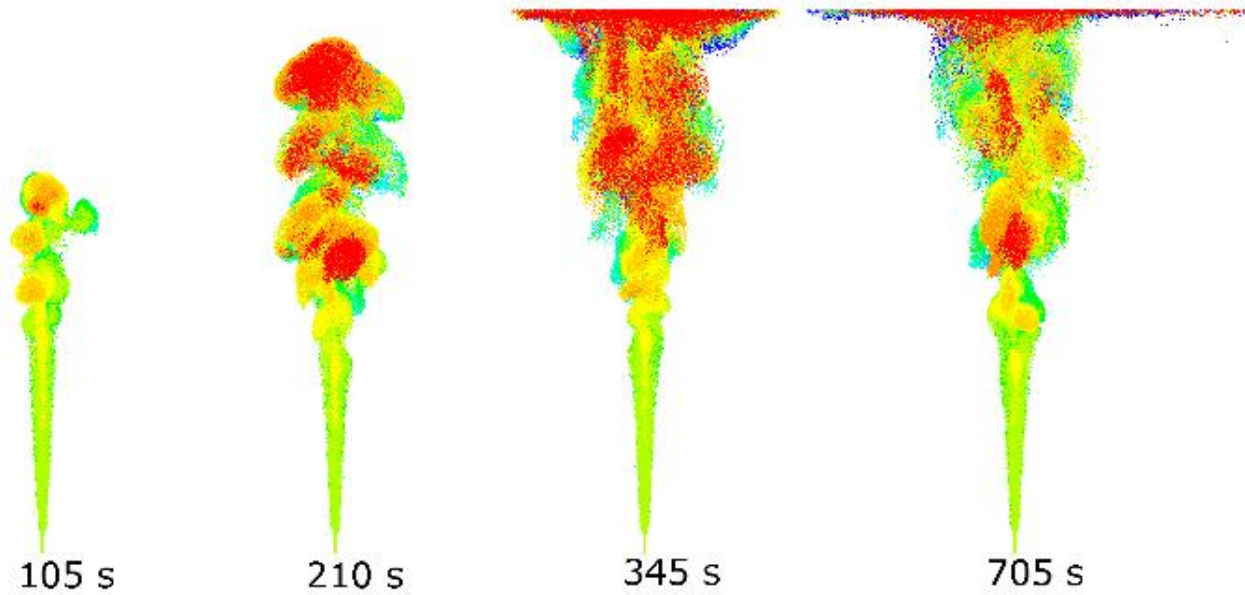


Figure 2: Development of the starting plume from 300 m at a constant rate of 30 kg/s.

Gas released from the ocean floor rises as bubbles towards the surface. If the release rate is sufficient, the buoyancy of the bubbles will cause the water to accelerate and travel upwards with bubbles. At the surface the bubbles enter the atmosphere whereas the water is forced outwards in a radial flow. The CFD model quantifies where and when bubbles penetrate the surface and the strength of the radial outflow.

Here we apply the CFD model for a selected release scenario and analyse the surfacing characteristics. The resulting surfacing fluxes and radial outflow velocity are compared to mathematical profiles to verify if some of these are representative for the *true* surfacing profiles.

MODEL DESCRIPTION

The CFD model developed to study large scale bubble plumes from subsea gas release is based on an Eulerian-Lagrangian modelling concept. The bubbles are treated as Lagrangian particles which move according to Newton's second law. The background fluid, i.e. the ocean, is governed by the Navier-Stokes equation in an Eulerian frame of reference. The interface between the ocean and the atmosphere is tracked by the *geo-reconstruct* algorithm. The details are provided in earlier publications (Olsen & Skjetne, 2016; Olsen *et al.*, 2017).

In a short summary it is worth mentioning that the model moves bubbles according to Newton's second law

$$\frac{d\mathbf{u}_b}{dt} = \frac{\mathbf{g}(\rho_b - \rho)}{\rho_b} + \mathbf{F}_D + \mathbf{F}_{VM} \quad (1)$$

where the forces on the right hand side are buoyancy, drag and virtual mass. The background fluids (ocean and atmosphere) are mathematically described by the principles of conservation of mass, momentum and energy through the continuity-, momentum- and heat-equation. The bubble motion and the flow of the background fluids are coupled through the drag term. Turbulence is modelled with a VLES model where

turbulent structures larger than the grid size are captured by the momentum equations and the subgrid turbulence is modelled by the k- ϵ model.

A model for the local mean bubble diameter is implemented accounting for break-up, coalescence, gas expansion and gas dissolution. Gas expansion is caused by the decrease in pressure and gas density as the bubbles rise upwards. Gas dissolution is driven by the difference in gas solubility and ocean saturation.

The model has been validated against meso scale experiments at 7, 30 and 50 meters depth and large scale data from 140 meters depth. The model is consistent with observations.

RESULTS

The modelling concept mentioned above was applied to a release of 30 kg/s of methane from a depth of 300 meters with an ocean temperature at 10°C and ocean salinity of 35 psu. The simulation results have been analysed to shed light on the surfacing mechanism and to discuss how these results can be reported as a boundary condition to atmospheric dispersion modelling.

The resulting plume from the release is illustrated in Figure 2 as predicted by the CFD simulation. Turbulent eddies with gas bubbles surface after roughly 4 minutes. The eddies cause a fluctuating surface rate and flux which would not have been captured by a RANS turbulence model. Observations of ocean bubble plumes confirms the fluctuating behaviour qualitatively. The surfacing rate is plotted in Figure 3. The surfacing rate (kg/s) is the area integral of the surface flux (kg/m²s). It averages at 1.6 kg/s indicating that gas dissolution is significant since only 5% of the released gas reaches the surface. The fluctuations are also significant.

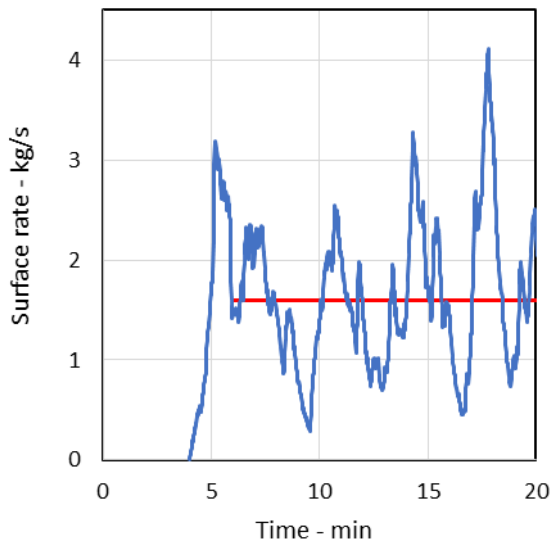


Figure 3: Surfacing rate as function of time, red line indicates average surfacing rate.

If we focus on the surfacing flux which varies in both time and space, we see that the fluctuations are even more significant. The resulting averaged surface flux using different averaging intervals are depicted in Figure 5 (next page). The two top plots are both with an averaging interval of 1 second, but from two different times (650 and 750 secs after release). There is a big difference in the peak flux and total surface rate between these two periods.

The flux is quite noisy. As the averaging interval increases, the flux distribution becomes more smooth and starts looking like a Gaussian distribution. Note that with an averaging period of 800 seconds the peak is less than ¼ of the maximum peaks in the fastest fluctuations. It is the long-averaged surface flux fitted to a Gaussian profile which is normally applied as a boundary condition in atmospheric dispersion modelling. This practice stems from modelling experiences with integral models and CFD models with RANS turbulence models. These models do not capture the fluctuations seen in Figures 3 and 5. Thus it can be questioned whether the conveniently long-averaged Gaussian profile is a proper boundary condition.

If we assume that a Gaussian profile is sufficiently representative of the surfacing flux, there are still some issues related on how to report the coefficients in the Gaussian expression. The Gaussian flux profile is given by

$$J = J_0 e^{-r^2/2\sigma^2} \quad (2)$$

where J_0 is the centre flux (or peak flux) and σ is the standard deviation. If the long-averaged surface flux is truly Gaussian, a perfect fit between the surface flux from

the CFD simulation and a Gaussian profile exists. This is unfortunately not true.

All gas surfacing within the radius defined by the standard deviation amount to 39% of all gas surfacing in total (see Appendix). By analysing the surface flux from the CFD simulation, the radius within which 39% of the gas surfaces can be extracted and reported as a standard deviation. Applying the principle that the Gaussian profile shall fulfil mass conservation, the centre flux is obtained from

$$\dot{m}_{tot} = 2\pi J_0 \sigma^2 \quad (3)$$

From this procedure we get $J_0=0.165 \text{ g/m}^2\text{s}$ and $\sigma=28 \text{ m}$. Alternatively we can quantify the coefficients by matching the Gaussian centre flux with the true peak flux and finding the standard deviation from mass conservation with Eq.(3). From this procedure we get $J_0=0.39 \text{ g/m}^2\text{s}$ and $\sigma=18 \text{ m}$. The true long-averaged profile and the Gaussian curve fits are plotted below in Figure 4.

The two procedures for obtaining the Gaussian coefficients obviously produces two quite different sets of coefficients. From this we can conclude that the profile is not truly Gaussian. For a true Gaussian, both procedures would have resulted in the same set of coefficients. This gives rise to an important question; which procedure provides the most representative Gaussian profile for the long-averaged surface flux? Visually it is probably the procedure based on the centre flux which seems superior (see Figure 5). However, it is also fair to question whether a Gaussian profile is truly representative

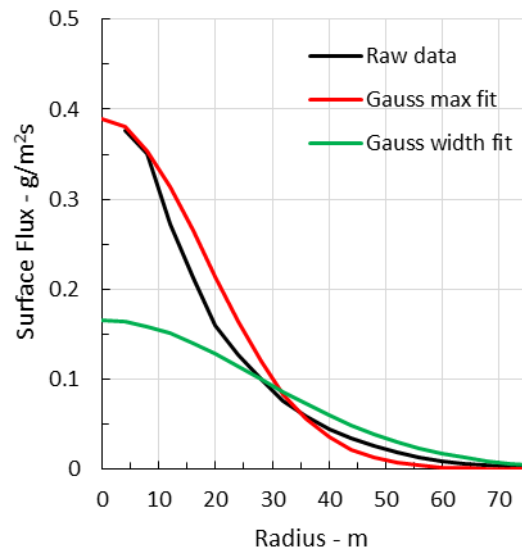
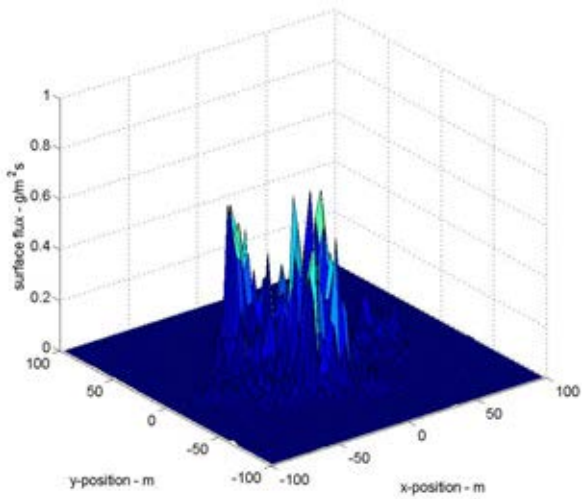
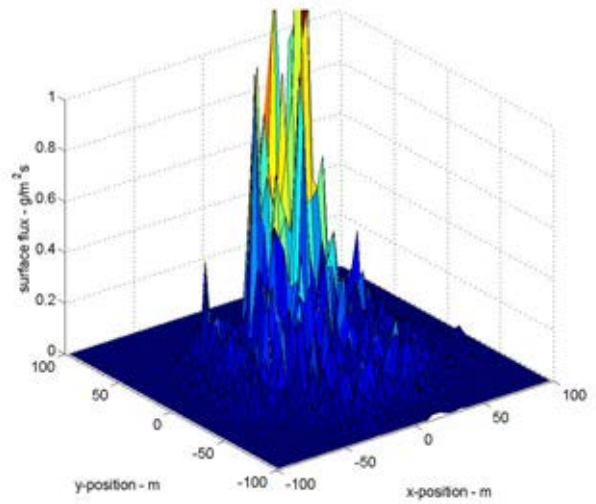


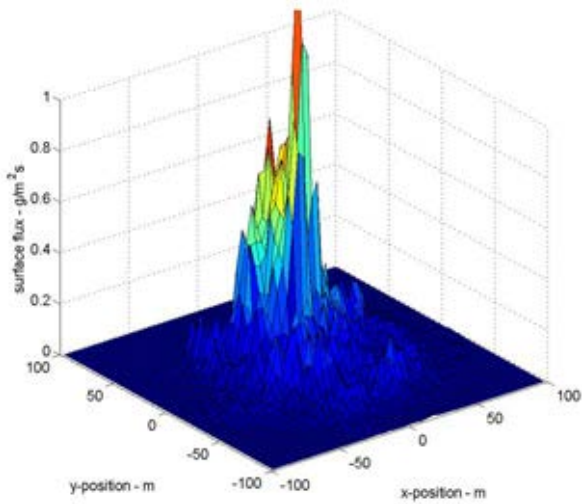
Figure 4: Surface flux



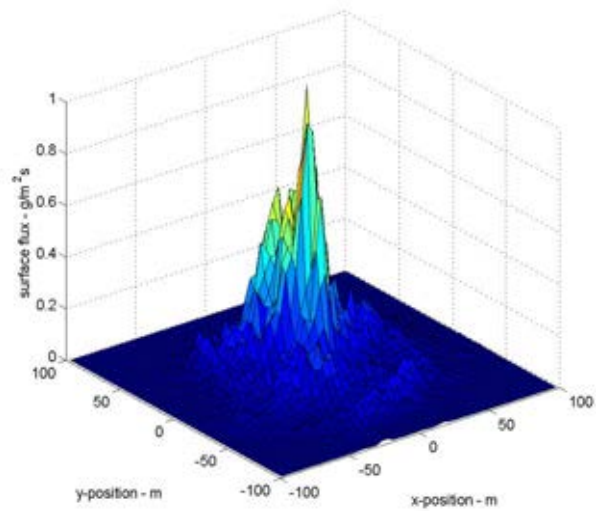
1 second averaging (at 750 secs)



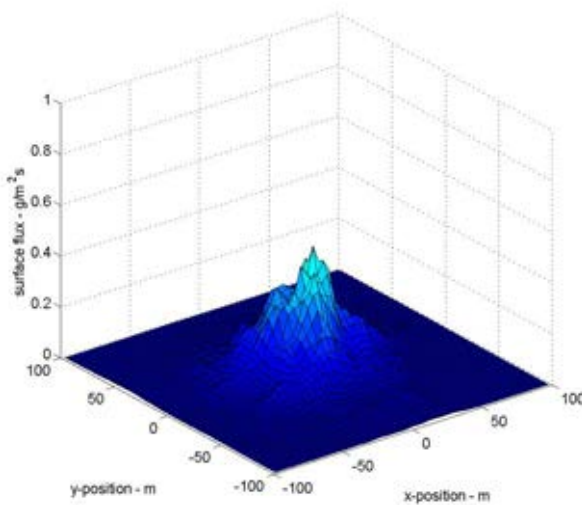
1 second averaging (at 650 secs)



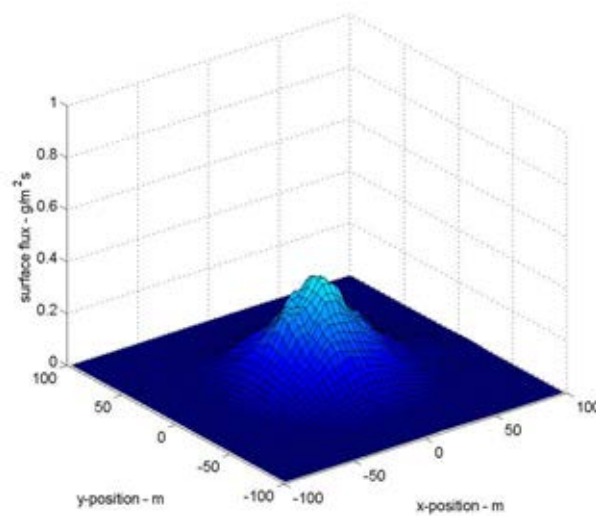
5 seconds averaging



10 seconds averaging



100 seconds averaging



800 seconds averaging

Figure 5: Surface flux for various averaging intervals. All averaging starts at 650 secs after start of release except top left example.

CONCLUSIONS

A CFD model with a transient VLES model representing turbulence has been applied to study the surfacing mechanism of an ocean plume caused by a subsea gas release. The resulting surface rate and surface flux is clearly fluctuating. A surface flux profile based on time-averaging over 800 seconds has a smooth shape which can be fitted to a Gaussian profile, although a perfect fit cannot be achieved. This indicates that the surface flux is not truly Gaussian even if similarities exist. Two different procedures for quantifying the Gaussian profile yields two different sets of Gaussian coefficients.

A consequence of these findings is to further study which profile best matches the true surface flux with respect to a risk assessment (e.g. conservatism). Sensitivity studies with atmospheric dispersion modelling could reveal the significance on how to report the surfacing profile. This includes assessments on both the fluctuating nature of the surfacing mechanism and the influence of how the time averaged profile is represented.

REFERENCES

- CLOETE, S., OLSEN, J.E., & SKJETNE, P. (2009). "CFD modeling of plume and free surface behavior resulting from a sub-sea gas release". *Applied Ocean Research*, **31**(3), 220-225.
- JOHANSEN, O. (2000). "DeepBlow - a Lagrangian plume model for deep water blowouts". *Spill Science & Technology Bulletin*, **6**(2), 103-111.
- MORTON, B.R., TAYLOR, G.I., & TURNER, J.S. (1956). "Turbulent gravitational convection from maintained and instantaneous sources". *Proc.Roy.Soc.A*, **234**, 171-178.
- OLSEN, J.E., & SKJETNE, P. (2016). "Modelling of underwater bubble plumes and gas dissolution with an Eulerian-Lagrangian CFD model". *Applied Ocean Research*, **59**, 193-200.
- OLSEN, J.E., SKJETNE, P., & JOHANSEN, S.T. (2017). "VLES turbulence model for an Eulerian-Lagrangian modeling concept for bubble plumes". *Applied Mathematical Modelling*, **000 Online**(1-11).
- ZHENG, L., & YAPA, P.D. (2002). "Modeling gas dissolution in deepwater oil/gas spills". *Journal of Marine Systems*, **31**, 299-309.

APPENDIX A

A Gaussian flux profile is given by

$$J = J_0 e^{-r^2/2\sigma^2} \quad (4)$$

The total gas rate through the entire surface is given by

$$\begin{aligned} \dot{m}_{\text{tot}} &= 2\pi \int_0^{\infty} J_0 e^{-\frac{r^2}{2\sigma^2}} r \, dr \\ &= 2\pi J_0 \left[-\sigma^2 e^{-\frac{r^2}{2\sigma^2}} \right]_0^{\infty} = 2\pi J_0 \sigma^2 \end{aligned} \quad (5)$$

The total gas rate through a surface limited by an outer radius R , is

$$\begin{aligned} \dot{m} &= 2\pi \int_0^R J_0 e^{-\frac{r^2}{2\sigma^2}} r \, dr \\ &= 2\pi J_0 \sigma^2 \left(1 - e^{-\frac{R^2}{2\sigma^2}} \right) \end{aligned} \quad (6)$$

The ratio of mass surfacing inside a radius R and the total mass is thus

$$\frac{\dot{m}}{\dot{m}_{\text{tot}}} = 1 - e^{-\frac{R^2}{2\sigma^2}} \quad (7)$$

The relative amount of gas surfacing within the radius defined by the standard deviation, $R = \sigma$, is thus

$$\frac{\dot{m}_{\sigma}}{\dot{m}_{\text{tot}}} = 1 - e^{-\frac{1}{2}} = 0.39 \quad (8)$$

This means that 39% of all gas surfaces within a radius equal to the standard deviation, and subsequently 86% within 2 standard deviations and 99% within 3 standard deviations. Bear in mind that this is only true if the surfacing profile is perfectly described by a Gaussian profile.

This might come as a surprise since some might believe that the amount represented by the distribution within the extent of the standard deviation is 68%. This number comes from statistics where they perform a straight integration of the profile without multiplying with r .

$$\frac{\int_0^{\sigma} e^{-\frac{r^2}{2\sigma^2}} \, dr}{\int_0^{\infty} e^{-\frac{r^2}{2\sigma^2}} \, dr} = 0.68 \quad (9)$$

This is in principle a 1D version of the above derivation which holds for a 2D case.